www.sciencemag.org/cgi/content/full/science.aae0061/DC1

Supplementary Materials for

Emergence of healing in the Antarctic ozone layer

Susan Solomon,* Diane J. Ivy, Doug Kinnison, Michael J. Mills, Ryan R. Neely III, Anja Schmidt

*Corresponding author. Email: solos@mit.edu

Published 30 June 2016 on *Science* First Release
DOI: 10.1126/science.aae0061

This PDF file includes:

Materials and Methods

I. Observations and Statistical Approach

Vertically resolved ozone abundances are from the ozonesonde stations of Syowa, Antarctica (69.0°S, 39.6°E) provided by the World Ozone and Ultraviolet Radiation Data Centre (WOUDC; woudc.org) along with South Pole, Antarctica (90.0°S) provided by the National Oceanic and Atmospheric Administration (NOAA; esrl.noaa.gov/gmd/dv/spo_oz). Total column Dobson ozone measurements are also taken from NOAA at the South Pole, available at the above web address. In some months, the sun is not high enough at the South Pole for accurate Dobson measurements. Therefore, the April through September South Pole total columns shown in Fig. S1 were obtained by integrating the measured ozonesonde abundances over the column. Only sondes that included data below 500 mbar and above 30 mbar were considered, and we present results only for months in which at least three sondings are available. Many more balloon sondes are typically available in September and October, greatly increasing the sampling in those months compared to others. We evaluated monthly mean profiles by two methods: 1) considering a grand average of all daily measurements with no adjustment for the residual column above the top of each balloon maximum ascent and 2) by extrapolating above the maximum level of each sonde using a scale height and then averaging. We found no significant difference in the trend between the two approaches for the key month of September.

Satellite total column data from the National Aeronautics and Space Administration's (NASA) Solar Backscatter Ultraviolet Merged Ozone Data set (SBUV, version 8.6, available at http://acd-ext.gsfc.nasa.gov/Data_services/merged/) were used to estimate polar cap averaged trends; the merged SBUV data is zonally averaged and provided at a resolution of 5° latitude. In certain months, the SBUV measurements do not extend all the way to the pole. Therefore, when the model simulations are compared to SBUV, the polar cap averaged total column data from WACCM were masked to cover the same area as SBUV by month. For the austral winter months, SBUV does not extend to 60°S, and in those months the polar cap averaged total column trends from the model were not masked and are indicated by the open bars in Figure 3.

The ozone hole areal extent (defined as the region with total ozone column less than 220 Dobson Units, per standard practice) was calculated from total column ozone data from NASA's Total

Ozone Mapping Spectrometer and Ozone Monitoring Instrument (TOMS/OMI, version 8, ozoneaq.gsfc.nasa.gov), which has a horizontal resolution of 1° latitude by 1.25° longitude for TOMS and a 1° latitude by 1° longitude for OMI. SBUV and Dobson data are considered to be accurately calibrated records for long-term trends *(19)*, while instrument instability is an issue for some of the TOMS record. The extent of the ozone hole was directly calculated by summing the area of grid cells with total column ozone less than 220 DU from 60-90°S. As TOMS/OMI data does not cover the pole in austral spring, this area was also added to the ozone hole extent. We do not interpolate or smooth the gridded SBUV or TOMS/OMI data, nor the model results. The day when the ozone hole reaches a threshold size of a given number of million km^2 is defined as the day when the ozone hole reached at least the given value and persisted above this threshold for at least the following 3 days (see Figure 5).

Some studies treat variability by using linear statistical fitting to factor out the influence of dynamical and other factors *(9,10)*, but it is not clear that statistical fits adequately capture the dependence of ozone on meteorological variables (which are themselves uncertain). Furthermore, feedbacks are expected between chemistry and meteorology, and these can display nonlinear behavior *(33)*. We employ the raw data without any fitting adjustments. The anomalous year 2002 is excluded from all trend analysis.

Trends were estimated by least-squares linear regression on each time series. The time periods presented for the trends are as up-to-date as practical within the limits of data availability. SBUV calibrated data were not yet available after 2014 at the time of writing of this paper; therefore trends for total ozone column depth and for vertical profiles are from 2000-2014. TOMS/OMI and ozonesonde data are available through 2015, and the trends of the ozone hole area are therefore from 2000-2015. The uncertainties on the trend estimates were calculated from the variance of the time series residuals and are provided at the 90% confidence interval. The 90% confidence interval (9 out of 10 odds) was chosen rather than 95% (19 out of 20) since only 14 or 15 years of data are available, and volcanic and other forms of variability can be expected to be poorly sampled.

II. The SD-WACCM Model The model used in this paper is the same as that employed in the detailed study of polar ozone chemistry described in *(24)*. Here we present information on the model formulation taken directly from that recent publication. The Community Earth System Model, version 1 (CESM1) is a coupled climate model for simulating the earth's climate system. CESM1 is composed of four separate component models simultaneously simulating the earth's atmosphere, ocean, land surface and sea-ice, and one central coupler component. The atmospheric component used in this study is the Whole-Atmosphere Community Climate Model, Version 4 (WACCM4), a comprehensive numerical model that spans the range of altitudes from the Earth's surface to the lower thermosphere. This version of WACCM is consistent with the Chemistry-Climate Model Intercomparison (CCMI) REFC1SD scenario *(38)*. We use the fixed dynamics SD-WACCM framework, with meteorological fields from the Modern Era Retrospective Analysis for Research and Applications (MERRA; *39*) through 2014 and from Goddard Earth Observing System operational data (GEOS) for 2015. A detailed comparison of MERRA and ERA-interim reanalyses insofar as polar heterogeneous chemistry is concerned showed good agreement after 2002 in the Antarctic, when Aqua and GEOS data both became available *(40)*. Comparisons between reanalysis temperature trends for 1980-2000 and

radiosondes, as well as lower stratospheric satellite temperatures suggested good agreement over that period *(41)*. However, Antarctic ozone depletion is extremely sensitive to absolute temperatures, as discussed in some detail in *(24),* and errors of as little as a degree could contribute to uncertainty in our simulations.

The chemical scheme of WACCM is based upon the chemical transport model Model of Ozone and Related Tracers (MOZART), *(42)*. It includes a detailed representation of neutral and ion chemistry needed to represent composition from the troposphere to the lower thermosphere. The chemical scheme includes the O_X, NO_X, HO_X, ClO_X, and BrO_X chemical families, along with gas phase and heterogeneous reactions on liquid binary and ternary sulfate polar stratospheric cloud particles, as well as solid nitric acid trihydrate and water ice polar stratospheric particles. A full range of industrial chlorocarbons and bromocarbons is included, along with natural sources such as CH_3Cl, CH_3Br, and several short-lived species such as bromoform *(42)*. The model includes 183 different species, 341 gas phase reactions, 114 photolytic processes, and 17 heterogeneous reactions on multiple aerosol types. The model has been shown to represent closely the satellite-observed seasonal evolution of Antarctic ozone loss as well as those of HCl and $ClONO_2$ *(24)*. The model slightly overestimates the absolute amount of winter Antarctic total ozone in the pre-depletion period, particularly in winter by about 20-30 DU (see Figure S1). Despite accurate calculation of the amount of springtime ozone loss as shown in *(24)*, starting from too much winter ozone is a primary factor in the 15% underestimate of the ozone hole size noted in the main text, since the ozone hole is defined based on a specific threshold value of 220 DU. Reactivities used for heterogeneous reactions are presented in Table 1 of *(24)*. The approach taken to calculating the distribution of PSCs ensures that both liquid and solid particles are present even under extreme cold temperatures in Antarctic winter. At model temperatures above ~200 K, liquid binary sulfate (LBS) is the only aerosol represented. In the calculations denoted CCMI in this paper, the LBS surface area density (SAD) used in the derivation of heterogeneous reaction rates is taken directly from the Chemistry Climate Model Initiative (CCMI) sulfate aerosol time series. CCMI provides aerosol observations through 2011, after which a repeating 1998/1999 monthly climatology was used. For all other calculations, the LBS surface area densities are taken from the modal aerosol model presented in *(26)* with explicit consideration of injection of sulfur dioxide from all significant and known volcanic eruptions over the period considered (see next section) along with non-volcanic background sources. As the model atmosphere cools below 200K, LBS aerosols swell, taking up HNO_3 and H_2O to give supercooled ternary solutions (STS).

The WACCM Aerosol Physical Chemistry Model (APCM) is used to derive the STS composition. The H_2SO_4 abundance used in APCM is derived from the observed or calculated sulfate SAD, respectively, from the CCMI data set or from the modal aerosol model. Nitric acid trihydrate (NAT) solid particles are also allowed to form. Observations suggest that a supersaturation of HNO_3 over NAT is needed before NAT can form. In all simulations in this study, the formation of NAT is assumed to occur at a supersaturation of 10, about 3K below its thermodynamic equilibrium temperature. The SAD and radius for STS and NAT assumes a lognormal size distribution with a width of 1.6. The number of particles cm^{-3} is set to 10 and 0.01 for STS and NAT respectively. An additional constraint to the STS and NAT microphysical approach is applied in which 20% of the total available HNO_3 is allowed to form NAT while the remaining 80% is available for STS. This essentially defines a nucleation approach consistent

with a "mix 2" PSC representation (see *(24)* and references therein). Following this approach yields gas-phase HNO_3 abundances that compare well to Aura MLS observations *(24)*, suggesting that the denitrification scheme is realistic.

Water-ice PSCs are also allowed to form. Here the underlying Community Atmospheric Model (CAM4) prognostic water approach derives and transports gas-phase, liquid-phase, and solid-phase water. The solid-phase water (i.e., water ice) is settled at the saturation condition of water vapor over ice, resulting in irreversible dehydration of the stratosphere. Following this approach, gas-phase water abundances compare well to Aura MLS observations, suggesting that the dehydration scheme is realistic. As in NAT and STS, the derived solid-phase water is used to derive the water ice SAD by assuming a lognormal size distribution, with a width of 1.6. In this study, the water-ice particle density was set to 0.1 particles cm^{-3}.

III. Volcanic and Background Aerosols We use volcanic and background aerosols taken directly from the work of *(26)* for the three post-2000 tests presented in this paper. That study presented a database of volcanic SO_2 emissions and plume altitudes for eruptions between 1990 and 2014, and used these along with other sources of sulfur (including OCS, anthropogenic SO_2, etc.) to simulate stratospheric sulfate aerosols in SD-WACCM. The database covers eruptions that have been detected by satellite instruments including Total Ozone Mapping Spectrometer (TOMS), Ozone Monitoring Instrument (OMI), Ozone Mapping and Profiler Suite (OMPS), Infrared Atmospheric Sounding Interferometer (IASI), Global Ozone Monitoring Experiment (GOME), Atmospheric Infrared Sounder (AIRS), Microwave Limb Sounder (MLS) and the Michelson Interferometer for Passive Atmospheric Sounding (MIPAS) instrument. Observations from MLS and other sources show that material from the 2015 eruption of Calbuco reached the stratosphere, and we updated our database using AIRS data for the Calbuco sulfur loading *(43, 44)*. The list of eruptions that are most relevant for Arctic and Antarctic ozone through 2015 is presented in table S1. For the volcanically clean case, only non-volcanic sources of stratospheric sulfur were included.

We employ the 3-mode version of the Modal Aerosol Model (MAM3, *26*) which represents internally mixed aerosols as three lognormal modes: Aitken, accumulation, and coarse. MAM3 is capable of representing complex interactions of aerosol particles, such as nucleation, condensation, coagulation, and sedimentation. The extension of MAM3 to include a new prognostic stratospheric aerosol option in WACCM is discussed in detail in *(26)*. Table S1 indicates estimated upper and lower altitude bounds on each eruption, and the mass is distributed evenly between those bounds. Injections into the troposphere are also included in the simulations (*26*), but those in the lower troposphere will have limited impact due to rainout; those that are close to the tropopause may be able to reach the stratosphere and are explicitly modeled. Our aerosol model has been shown to yield distributions of stratospheric aerosols that compare well to satellite data, as well as that from balloons and lidars *(26)*. We estimate the uncertainty in our modeled aerosols in the post-2005 volcanic period by comparing the calculated optical depths to lidar data as follows. We considered post-2005 lidar data from Mauna Loa, Tsukuba, Tomsk, and Ny Alesund for months in which there were at least 2 observations. Comparison of those data to the model monthly and zonally averaged values displayed a mean bias of 17% for 102 samples at Mauna Loa, 39% for 46 samples at Tsukuba, -12% for 68 samples at Tomsk, and 7.8% for 16 samples at Ny Alesund. Therefore, the mean model values show no bias error

greater than ±20% at 3 of the 4 stations, and an overall uncertainty estimate of ±40% is adopted here.

The complete time history of calculated aerosol properties is available on the Earth System Grid (http://dx.doi.org/10.5065/D6S180JM). Further model results presented in this paper are available on request to the WACCM liason, Michael Mills mmills@ucar.edu.

Table S1. Primary volcanic eruptions that could contribute to Arctic and Antarctic ozone changes since 1999. See the detailed table of datasets and references used to estimate emissions for each eruption through 2014 in Mills et al. (26, online supplement 5).

Volcano	Code	Year	Month	Day	SO_2 / Tg SO_2	Lat	Lon	Max plume height / km	Min plume height / km
Shishaldin	Sh	1999	3	13	0.06	54.8	196.0	13.7	11
Hekla	He	2000	2	26	0.2	64.0	340.3	12	11.3
Ruang	Ru	2002	9	25	0.06	2.3	125.4	20	18
Reventador	Rv	2002	11	3	0.1	-0.1	282.3	16.8	15
Anatahan	An	2003	5	10	0.07	16.4	145.7	15	14
Manam	Ma	2005	1	27	0.18	-4.1	145.0	19	18
Sierra Negra (Galápagos)	NS	2005	10	22	0.36	-0.8	268.8	15	14
Manam	Ma	2006	2	27	0.08	-4.1	145.0	12	2
Soufrière Hills	SH	2006	5	19	0.2	16.7	297.8	20	19
Rabaul (Tavurvur)	Ra	2006	10	7	0.23	-4.3	152.2	18	17
Llaima	Ll	2008	1	1	0.03	-38.7	288.3	12.5	3.7
Chaitén	Ch	2008	5	2	0.01	-42.8	287.4	21	7
Okmok	Ok	2008	7	12	0.12	53.4	191.9	16	10
Kasatochi	Ka	2008	8	8	1.7	52.2	184.5	18	10
Redoubt	Rd	2009	3	23	0.07	60.5	207.3	18.9	11
		2009	3	24	0.08	60.5	207.3	10	9
		2009	3	28	0.08	60.5	207.3	8	7
Sarychev Peak	Sa	2009	6	15	0.6	48.1	153.2	15	11
		2009	6	16	0.6	48.1	153.2	15	11
Merapi	Me	2010	11	8	0.44	-7.5	110.4	15.2	14
Grímsvötn	Gr	2011	5	21	0.07	64.4	342.7	20	15
		2011	5	22	0.2	64.4	342.7	15	10
		2011	5	23	0.3	64.4	342.7	10	5

Puyehue-Cordón Caulle	PC	2011	6	4	0.25	-40.6	287.9	13.7	12
Nabro	Na	2011	6	13	1.5	13.4	41.7	17	9.7
Kelut	Ke	2014	2	13	0.3	-7.9	112.3	26	17
Sangeang Api	SA	2014	5	30	0.1	-8.2	119.1	15.2	13.7
Calbuco	Ca	2015	4	23	0.4	-41.3	287.4	21	17.4

Table S2. Polar cap ozone trends and 90% confidence intervals over 2000-2014 (excluding 2002, see main text) from the SBUV observations, and for the three post-2000 model cases masked to SBUV coverage. Statistically significant trends are indicated in bold type. SBUV coverage in May, June, and July in the Southern Hemisphere does not extend to 63°S and the model data were not masked in those months.

SBUV mask 63-90S Trends (2000-2014) [DU/yr]

Month	chem-only		vol-clean		chem-dyn-vol		SBUV	
	Trend	*Error*	*Trend*	*Error*	*Trend*	*Error*	*Trend*	*Error*
Jan	**0.3**	**0.1**	**0.8**	**0.4**	**0.7**	**0.4**	0.3	0.3
Feb	**0.2**	**0.1**	**1.0**	**0.4**	**1.0**	**0.5**	**0.5**	**0.3**
Mar	0.1	0.1	**0.9**	**0.6**	**0.8**	**0.6**	0.5	0.5
Apr	0.1	0.1	0.4	0.5	0.3	0.6	-0.1	0.5
May	**0.2**	**0.1**	0.4	0.8	0.3	0.8	--	--
Jun	**0.2**	**0.1**	0.4	0.9	0.3	0.9	--	--
Jul	**0.3**	**0.1**	0.6	1.1	0.5	1.1	--	--
Aug	**0.8**	**0.1**	1.3	1.6	1.2	1.7	0.7	1.6
Sep	**1.3**	**0.1**	**3.0**	**1.6**	**2.8**	**1.6**	**2.5**	**1.7**
Oct	**1.1**	**0.1**	2.1	2.5	1.9	2.6	0.9	2.3
Nov	**0.8**	**0.1**	1.5	2.6	1.3	2.7	0.5	2.6
Dec	**0.6**	**0.1**	0.9	1.2	0.8	1.3	0.5	1.2

SBUV Mask 63-90N Trends (2000-2014) [DU/yr]

Month	chem-only		vol-clean		chem-dyn-vol		SBUV	
	Trend	*Error*	*Trend*	*Error*	*Trend*	*Error*	*Trend*	*Error*
Jan	**0.3**	**0.2**	-0.1	1.1	-0.2	1.1	-0.1	1.0
Feb	**0.5**	**0.3**	0.4	2.4	0.2	2.3	-0.3	2.1
Mar	0.2	0.2	0.5	2.5	0.3	2.4	-0.5	2.2
Apr	**0.3**	**0.2**	1.1	1.1	0.9	1.2	0.5	1.0
May	**0.3**	**0.2**	0.5	1.0	0.4	1.0	0.2	0.9
Jun	0.2	0.2	0.0	0.8	-0.1	0.8	-0.1	0.7
Jul	0.2	0.2	0.1	0.5	0.0	0.6	-0.1	0.6
Aug	0.1	0.2	0.3	0.4	0.2	0.5	0.2	0.4
Sep	0.2	0.2	**0.5**	**0.4**	0.4	0.5	0.4	0.5

Oct	0.3	0.3	**0.7**	**0.5**	0.5	0.6	0.4	0.5
Nov	0.0	0.2	0.0	0.8	-0.2	0.7	-0.4	0.6
Dec	**0.3**	**0.2**	-0.5	0.9	-0.6	0.8	**-0.9**	**0.7**

Table S3. South Pole ozone trends and 90% confidence intervals over 2000-2014 (excluding 2002, see main text) from data at the station and for the three model cases for 85-90°S. Observations in April through September are taken from ozonesondes and are indicated in red, while data for January, February, October, November and December are from Dobson measurements. Statistically significant trends are indicated in bold type.

South Pole Trends (2000-2014) [DU/yr]

Month	85-90S chem-only		85-90S vol-clean		85-90S chem-dyn-vol		South Pole Data	
	Trend	*Error*	*Trend*	*Error*	*Trend*	*Error*	*Trend*	*Error*
January	**0.3**	**0.1**	**1.5**	**0.7**	**1.4**	**0.7**	**1.5**	**0.8**
February	**0.2**	**0.1**	**1.5**	**1.2**	**1.4**	**1.1**	**1.8**	**1.4**
March	**0.2**	**0.1**	0.5	1.0	0.4	1.0	**0.8**	**0.6**
April	0.1	0.1	**0.9**	**0.9**	0.8	0.8	1.0	1.8
May	**0.2**	**0.1**	0.1	1.2	0.0	1.2	0.3	1.3
June	**0.2**	**0.1**	0.2	1.4	0.2	1.3	1.5	1.8
July	**0.2**	**0.1**	-0.5	1.4	-0.5	1.4	1.1	2.5
August	**0.5**	**0.1**	0.3	1.7	0.2	1.8	1.3	2.5
September	**1.3**	**0.1**	**2.0**	**1.5**	**1.9**	**1.5**	**2.5**	**1.5**
October	**1.2**	**0.1**	2.3	2.7	2.1	2.9	1.6	3.0
November	**1.0**	**0.1**	1.9	4.9	1.7	5.0	1.6	5.6
December	**0.6**	**0.2**	1.1	2.3	1.0	2.4	1.0	2.6

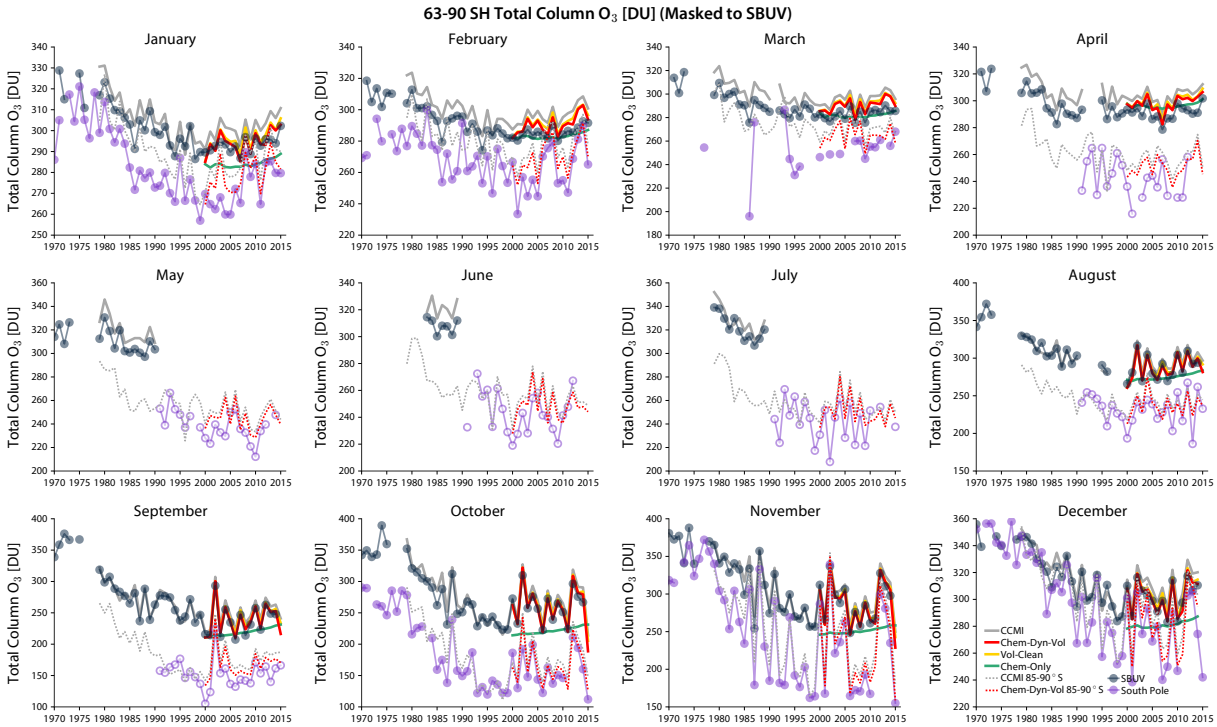

Fig. S1. Monthly averaged Antarctic total ozone column for all months, from SBUV and South Pole observations and for a series of model calculations. Total ozone data at the geographic South Pole are from Dobson observations where available (filled circles) and balloon sondes (open circles, for April-September, when there is not sufficient sunlight for the Dobson). SBUV data for each month are compared to model runs averaged over the polar cap latitude band accessible by the instrument, while South Pole data are compared to simulations for 85-90°S. SBUV coverage does not extend into the polar cap in some winter months.

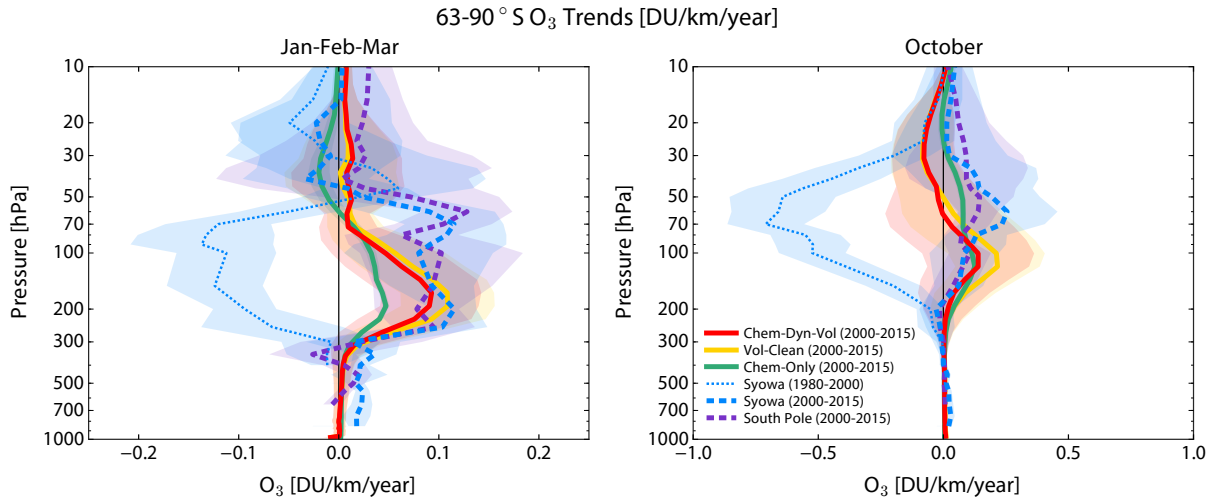

Fig. S2. Trends in January-February-March and October averaged ozone profiles from balloons at the South Pole and Syowa (69°S, 39.58°E) stations versus pressure for 2000-2015 (excluding 2002, see main text) along with model simulations averaged over the polar cap for the chem-dyn-vol, vol-clean, and chem-only model simulations. The trends from Syowa for 1980-2000 are also shown for comparison. The shading represents the uncertainties on the trends at the 90% statistical confidence interval.

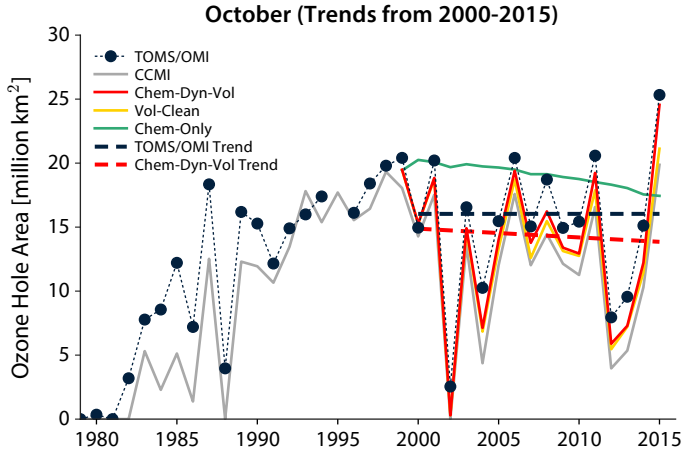

Fig. S3. Annual size of the October monthly average ozone hole (defined as the region where total ozone amount is less than 220 DU) from TOMS/OMI satellite observations together with numerical model simulations for the chem-dyn-vol, vol-clean, and chem-only simulations. Trends from 2000-2015 (excluding 2002, see main text) in the TOMS/OMI observations and the chem-dyn-vol model calculations are indicated by heavy dashed lines, but are not significant at 90% confidence.

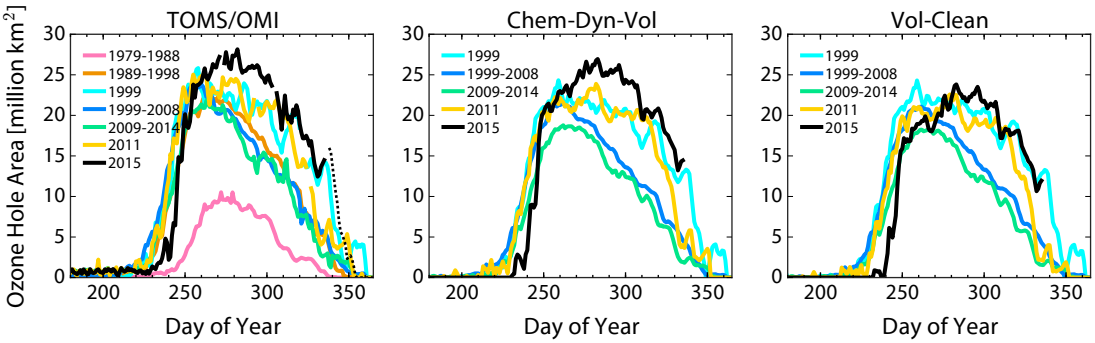

Fig. S4. Daily measurements (left) and chem-dyn-vol model calculations (center) as well as vol-clean calculations (right) of the size of the Antarctic ozone hole versus day of year in different time intervals and years, with 2015 shown in black and 2011 in yellow. Both 2011 and 2015 were perturbed by volcanic eruptions and display extremely large ozone holes in October compared to most other years, with 2015 being a clear and sustained record in October only when the volcanic perturbation is considered (center). Dashed black line denotes TOMS/OMI data after the period covered by the model runs.

References and Notes

1. J. C. Farman, B. G. Gardiner, J. D. Shanklin, Large losses of total ozone in Antarctica reveal seasonal ClO_x/NO_x interaction. *Nature* **315**, 207–210 (1985). doi:10.1038/315207a0

2. World Meteorological Organization/United Nations Environment Programme (WMO/UNEP), *Scientific Assessment of Ozone Depletion: 2014* (Global Ozone Research and Monitoring Project Report No. 55, WMO, 2014).

3. D. J. Hofmann, S. J. Oltmans, J. M. Harris, B. J. Johnson, J. A. Lathrop, Ten years of ozonesonde measurements at the south pole: Implications for recovery of springtime Antarctic ozone. *J. Geophys. Res.* **102**, 8931–8943 (1997). doi:10.1029/96JD03749

4. M. J. Newchurch, E.-S. Yang, D. M. Cunnold, G. C. Reinsel, J. M. Zawodny, J. M. Russell III, Evidence for slowdown in stratospheric ozone loss: First stage of ozone recovery. *J. Geophys. Res.* **108**, 4507 (2003). doi:10.1029/2003JD003471

5. N. R. P. Harris, B. Hassler, F. Tummon, G. E. Bodeker, D. Hubert, I. Petropavlovskikh, W. Steinbrecht, J. Anderson, P. K. Bhartia, C. D. Boone, A. Bourassa, S. M. Davis, D. Degenstein, A. Delcloo, S. M. Frith, L. Froidevaux, S. Godin-Beekmann, N. Jones, M. J. Kurylo, E. Kyrölä, M. Laine, S. T. Leblanc, J.-C. Lambert, B. Liley, E. Mahieu, A. Maycock, M. de Mazière, A. Parrish, R. Querel, K. H. Rosenlof, C. Roth, C. Sioris, J. Staehelin, R. S. Stolarski, R. Stübi, J. Tamminen, C. Vigouroux, K. A. Walker, H. J. Wang, J. Wild, J. M. Zawodny, Past changes in the vertical distribution of ozone – Part 3: Analysis and interpretation of trends. *Atmos. Chem. Phys.* **15**, 9965–9982 (2015). doi:10.5194/acp-15-9965-2015

6. F. Tummon, B. Hassler, N. R. P. Harris, J. Staehelin, W. Steinbrecht, J. Anderson, G. E. Bodeker, A. Bourassa, S. M. Davis, D. Degenstein, S. M. Frith, L. Froidevaux, E. Kyrölä, M. Laine, C. Long, A. A. Penckwitt, C. E. Sioris, K. H. Rosenlof, C. Roth, H.-J. Wang, J. Wild, Intercomparison of vertically resolved merged satellite ozone data sets: Interannual variability and long-term trends. *Atmos. Chem. Phys.* **15**, 3021–3043 (2015). doi:10.5194/acp-15-3021-2015

7. T. G. Shepherd, D. A. Plummer, J. F. Scinocca, M. I. Hegglin, V. E. Fioletov, M. C. Reader, E. Remsberg, T. von Clarmann, H. J. Wang, Reconciliation of halogen-induced ozone loss with the total column ozone record. *Nat. Geosci.* **7**, 443–449 (2014). doi:10.1038/ngeo2155

8. E.-S. Yang, D. M. Cunnold, M. J. Newchurch, R. J. Salawitch, M. P. McCormick, J. M. Russell III, J. M. Zawodny, S. J. Oltmans, First stage of Antarctic ozone recovery. *J. Geophys. Res.* **113**, D20308 (2008). doi:10.1029/2007JD009675

9. M. L. Salby, E. Titova, L. Deschamps, Rebound of Antarctic ozone. *Geophys. Res. Lett.* **38**, L09702 (2011). doi:10.1029/2011GL047266

10. J. Kuttippurath, F. Lefèvre, J.-P. Pommereau, H. K. Roscoe, F. Goutail, A. Pazmiño, J. D. Shanklin, Antarctic ozone loss in 1979–2010: First sign of ozone recovery. *Atmos. Chem. Phys.* **13**, 1625–1635 (2013). doi:10.5194/acp-13-1625-2013

11. WMO, "WMO Antarctic Ozone Bulletins: 2015," 2015; www.wmo.int/pages/prog/arep/WMOAntarcticOzoneBulletins2015.html.

12. S. Solomon, Stratospheric ozone depletion: A review of concepts and history. *Rev. Geophys.* **37**, 275–316 (1999). doi:10.1029/1999RG900008

13. J. Kuttippurath, S. Godin-Beekmann, F. Lefèvre, M. L. Santee, L. Froidevaux, A. Hauchecorne, Variability in Antarctic ozone loss in the last decade (2004–2013): High-resolution simulations compared to Aura MLS observations. *Atmos. Chem. Phys.* **15**, 10385–10397 (2015). doi:10.5194/acp-15-10385-2015

14. N. J. Livesey, M. L. Santee, G. L. Manney, A Match-based approach to the estimation of polar stratospheric ozone loss using Aura Microwave Limb Sounder observations. *Atmos. Chem. Phys.* **15**, 9945–9963 (2015). doi:10.5194/acp-15-9945-2015

15. D. J. Hofmann, S. J. Oltmans, Antarctic ozone during 1992: Evidence for Pinatubo volcanic aerosol effects. *J. Geophys. Res.* **98**, 18555–18561 (1993). doi:10.1029/93JD02092

16. R. W. Portmann, S. Solomon, R. R. Garcia, L. W. Thomason, L. R. Poole, M. P. McCormick, Role of aerosol variations in anthropogenic ozone depletion in the polar regions. *J. Geophys. Res.* **101**, 22991–23006 (1996). doi:10.1029/96JD02608

17. J.-P. Vernier, L. W. Thomason, J.-P. Pommereau, A. Bourassa, J. Pelon, A. Garnier, A. Hauchecorne, L. Blanot, C. Trepte, D. Degenstein, F. Vargas, Major influence of tropical volcanic eruptions on the stratospheric aerosol layer during the last decade. *Geophys. Res. Lett.* **38**, L12807 (2011). doi:10.1029/2011GL047563

18. C. Brühl, J. Lelieveld, H. Tost, M. Höpfner, N. Glatthor, Stratospheric sulfur and its implications for radiative forcing simulated by the chemistry climate model EMAC. *J. Geophys. Res. Atmos.* **120**, 2103–2118 (2015). Medline doi:10.1002/2014JD022430

19. R. D. McPeters, P. K. Bhartia, D. Haffner, G. L. Labow, L. Flynn, The version 8.6 SBUV ozone data record: An overview. *J. Geophys. Res.* **118**, 8032–8039 (2013).

20. W. Chehade, M. Weber, J. P. Burrows, Total ozone trends and variability during 1979–2012 from merged data sets of various satellites. *Atmos. Chem. Phys.* **14**, 7059–7074 (2014). doi:10.5194/acp-14-7059-2014

21. D. R. Marsh, M. J. Mills, D. E. Kinnison, J.-F. Lamarque, N. Calvo, L. M. Polvani, Climate change from 1850 to 2005 simulated in CESM1(WACCM). *J. Clim.* **26**, 7372–7391 (2013). doi:10.1175/JCLI-D-12-00558.1

22. A. Kunz, L. L. Pan, P. Konopka, D. E. Kinnison, S. Tilmes, Chemical and dynamical discontinuity at the extratropical tropopause based on START08 and WACCM analyses. *J. Geophys. Res.* **116**, D24302 (2011). doi:10.1029/2011JD016686

23. Materials and methods are available as supplementary materials on *Science* Online.

24. S. Solomon, D. Kinnison, J. Bandoro, R. R. Garcia, Polar ozone depletion: An update. *J. Geophys. Res.* **120**, 7958–7974 (2015).

25. F. Arfeuille, B. P. Luo, P. Heckendorn, D. Weisenstein, J. X. Sheng, E. Rozanov, M. Schraner, S. Brönnimann, L. W. Thomason, T. Peter, Modeling the stratospheric warming following the Mt. Pinatubo eruption: Uncertainties in aerosol extinction. *Atmos. Chem. Phys.* **13**, 11221–11234 (2013). doi:10.5194/acp-13-11221-2013

26. M. J. Mills, A. Schmidt, R. Easter, S. Solomon, D. E. Kinnison, S. J. Ghan, R. R. Neely III, D. R. Marsh, A. Conley, C. G. Bardeen, A. Gettelman, Global volcanic aerosol properties derived from emissions, 1990-2014, using WACCM5. *J. Geophys. Res.* **121**, 2332–2348 (2015).

27. M. Höpfner, C. D. Boone, B. Funke, N. Glatthor, U. Grabowski, A. Günther, S. Kellmann, M. Kiefer, A. Linden, S. Lossow, H. C. Pumphrey, W. G. Read, A. Roiger, G. Stiller, H. Schlager, T. von Clarmann, K. Wissmüller Sulfur dioxide (SO_2) from MIPAS in the upper troposphere and lower stratosphere 2002–2012. *Atmos. Chem. Phys.* **15**, 7017–7037 (2015). doi:10.5194/acp-15-7017-2015

28. P. A. Newman, E. R. Nash, S. R. Kawa, S. A. Montzka, S. M. Schauffler, When will the Antarctic ozone hole recover? *Geophys. Res. Lett.* **33**, L12814 (2006). doi:10.1029/2005GL025232

29. A. A. Scaife, D. R. Jackson, R. Swinbank, N. Butchart, H. E. Thornton, M. Keil, L. Henderson, Stratospheric vacillations and the major warming over Antarctica in 2002. *J. Atmos. Sci.* **62**, 629–639 (2005). doi:10.1175/JAS-3334.1

30. P. M. Forster, R. S. Freckleton, K. P. Shine, On aspects of the concept of radiative forcing. *Clim. Dyn.* **13**, 547–560 (1997). doi:10.1007/s003820050182

31. B. Hassler, G. E. Bodeker, S. Solomon, P. J. Young, Changes in the polar vortex: Effects on Antarctic total ozone observations at various stations. *Geophys. Res. Lett.* **38**, L01805 (2011). doi:10.1029/2010GL045542

32. A. Tabazadeh, K. Drdla, M. R. Schoeberl, P. Hamill, O. B. Toon, Arctic "ozone hole" in a cold volcanic stratosphere. *Proc. Natl. Acad. Sci. U.S.A.* **99**, 2609–2612 (2002). Medline doi:10.1073/pnas.052518199

33. S. Meul, S. Oberländer-Hayn, J. Abalichin, U. Langematz, Nonlinear response of modeled stratospheric ozone to changes in greenhouse gases and ozone depleting substances in the recent past. *Atmos. Chem. Phys.* **15**, 6897–6911 (2015). doi:10.5194/acp-15-6897-2015

34. P. Braesicke, J. Keeble, X. Yang, G. Stiller, S. Kellmann, N. L. Abraham, A. Archibald, P. Telford, J. A. Pyle, Circulation anomalies in the Southern Hemisphere and ozone changes. *Atmos. Chem. Phys.* **13**, 10677–10688 (2013). doi:10.5194/acp-13-10677-2013

35. F. Li, J. Austin, J. Wilson, The strength of the Brewer–Dobson circulation in a changing climate: Coupled chemistry–climate model simulations. *J. Clim.* **21**, 40–57 (2008). doi:10.1175/2007JCLI1663.1

36. C. McLandress, T. G. Shepherd, Simulated anthropogenic changes in the Brewer–Dobson Circulation, including its extension to high latitudes. *J. Clim.* **22**, 1516–1540 (2009). doi:10.1175/2008JCLI2679.1

37. N. Butchart, The Brewer-Dobson circulation. *Rev. Geophys.* **52**, 157–184 (2014). doi:10.1002/2013RG000448

38. V. Eyring, J.-F. Lamarque, P. Hess, F. Arfeuille, K. Bowman, M. P. Chipperfield, B. Duncan, A. Fiore, A. Gettelman, M. A. Giorgetta, C. Granier, M. Hegglin, D. Kinnison, M. Kunze, U. Langematz, B. Luo, R. Martin, K. Matthes, P. A. Newman, T. Peter, A. Robock, T. Ryerson, A. Saiz-Lopez, R. Salawitch, M. Schultz, T. G. Shepherd, D.

Shindell, J. Stähelin, S. Tegtmeier, L. Thomason, S. Tilmes, J.-P. Vernier, D. W. Waugh, P. J. Young, Overview of IGAC/SPARC Chemistry-Climate Model Initiative (CCMI) Community Simulations in Support of Upcoming Ozone and Climate Assessments. *SPARC Newsl.* **40**, 48–66 (2013).

39. M. M. Rienecker, M. J. Suarez, R. Gelaro, R. Todling, J. Bacmeister, E. Liu, M. G. Bosilovich, S. D. Schubert, L. Takacs, G.-K. Kim, S. Bloom, J. Chen, D. Collins, A. Conaty, A. da Silva, W. Gu, J. Joiner, R. D. Koster, R. Lucchesi, A. Molod, T. Owens, S. Pawson, P. Pegion, C. R. Redder, R. Reichle, F. R. Robertson, A. G. Ruddick, M. Sienkiewicz, J. Woollen, MERRA: NASA's Modern-Era Retrospective Analysis for Research and Applications. *J. Clim.* **24**, 3624–3648 (2011). doi:10.1175/JCLI-D-11-00015.1

40. Z. D. Lawrence, G. L. Manney, K. Minschwaner, M. L. Santee, A. Lambert, Comparisons of polar processing diagnostics from 34 years of the ERA-Interim and MERRA reanalyses. *Atmos. Chem. Phys.* **15**, 3873–3892 (2015). doi:10.5194/acp-15-3873-2015

41. D. Ivy, S. Solomon, H. E. Rieder, Radiative and dynamical influences on polar stratospheric temperature trends. *J. Clim.*, 10.1175/JCLI-D-15-0503.1 (2015). doi:10.1175/JCLI-D-15-0503.1

42. D. E. Kinnison, G. P. Brasseur, S. Walters, R. R. Garcia, D. R. Marsh, F. Sassi, V. L. Harvey, C. E. Randall, L. Emmons, J. F. Lamarque, P. Hess, J. J. Orlando, X. X. Tie, W. Randel, L. L. Pan, A. Gettelman, C. Granier, T. Diehl, U. Niemeier, A. J. Simmons, Sensitivity of chemical tracers to meteorological parameters in the MOZART-3 chemical transport model. *J. Geophys. Res.* **112**, D20302 (2007). doi:10.1029/2006JD007879

43. J. E. Romero, D. Morgavi, F. Arzilli, R. Daga, A. Caselli, F. Reckziegel, J. Viramonte, J. Díaz-Alvarado, M. Polacci, M. Burton, D. Perugini, Eruption dynamics of the 22–23 April 2015 Calbuco Volcano (Southern Chile): Analysis of tephra fall deposits. *J. Volcanol. Geotherm. Res.* **317**, 15–29 (2016). doi:10.1016/j.jvolgeores.2016.02.027

44. Nicarnica Aviation, "Cabulco eruption, April 2015: AIRS Satellite Measurements," 24 April 2015; http://nicarnicaaviation.com/calbuco-eruption-april-2015/#2.